IOP Conference Series: Earth and Environmental Science

PAPER • **OPEN ACCESS**

Research on Microstructure and Properties of 304 Stainless Steel Made by MIG Filler Additive Manufacturing

To cite this article: Yishan Bai *et al* 2019 *IOP Conf. Ser.: Earth Environ. Sci.* **237** 032096

IOP Conf. Series: Earth and Environmental Science **237** (2019) 032096 doi:10.1088/1755-1315/237/3/032096

Research on Microstructure and Properties of 304 Stainless Steel Made by MIG Filler Additive Manufacturing

Yishan Bai[1], Qingwei Gao[1], Xin Chen[1], Hao Yin[1], Longfei Fang[1] and Jian Zhao[1*]

[1]College of Materials Engineering, Shanghai University of Engineering Science, Shanghai 201620, China

[*]Corresponding author's e-mail: zhaojianhit@163.com

Abstract. In this paper, the MIG wire-filling method was used to fabricate 304 stainless steel in a layer-by-layer filling manner on a 20 mm thick low carbon steel surface. The microstructures of the upper, middle and lower parts of the cladding layer under different heat input conditions were studied. Finally, the microhardness test was carried out on different heights of the cladding layer produced by additive manufacturing under different processes. The results showed that with the gradual reduction of heat input, the grains of the same characteristic area were gradually refined under different processes. The cladding layer structure was mainly composed of columnar crystals, dendrites and equiaxed crystals. The microhardness increased as the heat input decreased. In this paper, the highest hardness value was 257.8 HV. The process parameters were voltage 27 V, current 190 A, deposition speed 8.69 mm/s, wire feeding speed 7 m/min, wire feeding angle 90° and shielding gas flow rate 15 L/min, respectively.

1. Introduction

The traditional manufacturing technology of metal parts mainly focused on casting and forging. However, the shape of the mold limited the production of complex structural parts and the extensive use of cutting technology in the forging process resulted in material waste. Additive manufacturing, as a kind of based on the digital model by adding material accumulated step by step, forming the integration of manufacturing technology in the manufacturing process, production cost and production cycle had great advantages, and this method could realize complex geometry customization, eliminate the restrictions of traditional model, and be applied in the aerospace, biomedical, automobile industry and other industries[1-5]. At present, research on additive manufacturing mainly focused on arc, laser and electron beam, etc. Laser and electron beam were high-energy beam additive manufacturing technologies with the advantages of precise energy control, but the manufacturing cost was high and the equipment was expensive[6-8]. In contrast, arc additive manufacturing had been widely studied for its high density, excellent mechanical properties, good metallurgical bonding, uniform chemical composition, and complex shape manufacturing[9]. However, the arc energy could not be precisely controlled, so the heat accumulated in the additive manufacturing process had an adverse effect on the microstructure and its forming accuracy[10]. Therefore, the MIG wire filling process parameters on the increase of material in the process of manufacturing cladding layer of forming quality was great significance.

In this paper, the effects of different heat input conditions on the microstructure and properties of the cladding layer of 304 stainless steel MIG filler wire were studied, and the process and theoretical guidance for the MIG wire filler manufacturing technology of the subsequent metal materials were provided.

2. Experiment

The test used 20 mm thick mild steel mother material and 304 stainless steel welding wire with diameter of 1.2 mm. The chemical composition of welding wire was shown in table 1. Before the test, the oxide film and oil on the surface of low carbon steel base material were removed by mechanical grinding. Then, the surface of the workpiece was cleaned with anhydrous ethanol.

Table 1. Chemical composition of welding wire (wt. %).

C	Si	Mn	S	Cr	Ni	P	Fe
0.055	0.60	1.00	0.005	18.20	8.43	0.027	bal

In this experiment, a MIG welding machine manufactured by CLOOS of Germany, model QINEO STEP 350 C, was used to send Ar gas with a gas flow of 15 L/min to the cladding layer in the process of additive manufacturing through the welding gun, isolating the surrounding air into the arc area when the arc and matrix react. The specific technological parameters adopted in this experiment were shown in table 2. As the wire feeding speed and current change synchronously in arc welding, different line energy could be obtained by changing the deposition speed. The one-direction additive manufacturing test was carried out using MIG filler. When the first cladding layer was finished, the nozzle was moved up by the height of one cladding layer and the next cladding layer was manufactured. The cladding layers obtained by 5 different technological parameters were all three layers and the height of each cladding layer was about 2 mm. In the increase of material in the manufacturing process using the thermometer interpass temperature control at about 70℃, constant wire feeding angle for 90°, wire extension was 2 cm, arc length was 1 cm.

Table 2. Welding process parameters.

Samples	Welding voltage(V)	Welding current(A)	Deposition velocity(mm/s)	Wire feed rate(m/min)	Heat input (J/mm)	Gas flow (L/min)
1	27	190	4.47	7	1147.7	15
2	27	190	6.09	7	842.4	15
3	27	190	7.25	7	707.6	15
4	27	190	8.69	7	590.3	15
5	27	190	9.67	7	530.5	15

After welding, DK7730C spark-wire cutter was used to cut the stable section in the middle of the cladding layer to prepare the sample under 5 different technological parameters, and the weld section was ground to #1200 with sandpaper and polished. $CuSO_4$: HCl: H_2O ratio of 4g: 20ml: 20ml hydrochloric acid solution was used to corrode the cross section, and then metallographic analysis was conducted on the cross section of the cladding layer. The HXD-1000 microhardness tester was used to test the hardness of each cladding sample from the top of the cladding layer. The hardness was measured successively at 1 mm intervals along the center line to the parent material. The load was 300 g and the continuous loading time was 15 s. The dotting schematic was shown in figure 1.

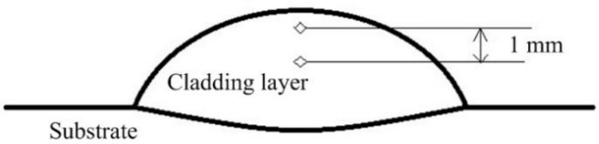

Figure 1. Cladding layer microhardness test position diagram.

3. Results and Discussion

3.1. Macro morphology of the cladding layer

The process parameters shown in table 2 were used to carry out the additive manufacturing process test. The morphology of the five groups of the cladding layer showed certain commonness, mainly reflected in the highest starting height of the cladding layer, the moderate height of the middle stable part, the uniform and even size, and the lowest end height. The difference in macroscopic morphology was mainly reflected in two aspects. The difference in macroscopic morphology was mainly reflected in two aspects. On the one hand, at the beginning of additive manufacturing, the energy gradually increased according to the characteristics of the arc power source and the melted wire gradually increased. The energy reached the maximum value and enters the stable state, so the amount of molten wire was relatively uniform. The arc energy gradually decreased as it entered the late stage of additive manufacturing. The amount of wire fed according to the characteristics of the power supply was also reduced, so the amount of melted wire at the end is the least and the height of the cladding layer was the lowest. On the other hand, due to the arc's mining effect on the molten pool, the molten liquid metal will be discharged to the rear area of the molten pool, and some liquid metals will be thrown to the rear of the molten pool and immediately solidify, resulting in a significant increase in the size of the initial end of the cladding layer[11]. The principle was shown in figure 2.

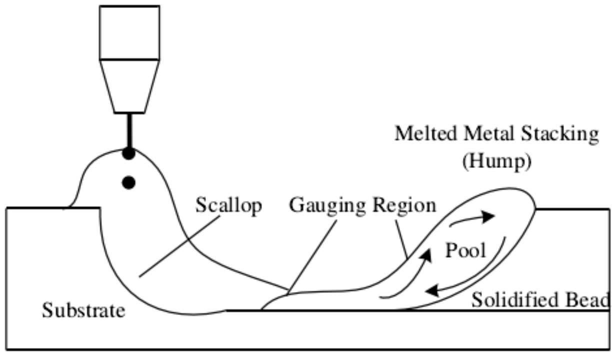

Figure 2. Impact of arc on molten pool[11].

3.2. Microstructure analysis of cladding layer

The microstructure of five characteristic regions of cladding layer (lower, middle, interlayer and upper) under different line energy was observed. Figure 3 showed that the microstructure of the bottom of the cladding layer under different thermal inputs, from which it could be seen that there was a clear fusion line between the matrix and the first cladding layer in the five samples. It could be seen that the metallurgical bond was formed between the cladding layer and the base metal. The first cladding layer of the five samples grew in the shape of a columnar crystal along the direction perpendicular to the fusion line to the inside of the cladding layer. This was because in the initial stage of solidification of the molten pool, the temperature gradient between the bottom of the molten pool and the base metal was large, and the solidification rate R tends to zero, and G/R tended to infinity, where G was the liquidus temperature gradient. At this time, it grows from the base metal outward in a planar crystal. With the effect of heat conduction, the temperature of the base metal raised, and the liquid molten pool was no longer a low-temperature base metal, but a relatively high-temperature planar crystal. The plate thickness selected herein was large and the cooling rate was fast, resulting in the growth of the part in the form of columnar crystals. It could be seen that as the line energy was gradually lowered, the grain size of sample 1 to sample 5 was gradually fine.

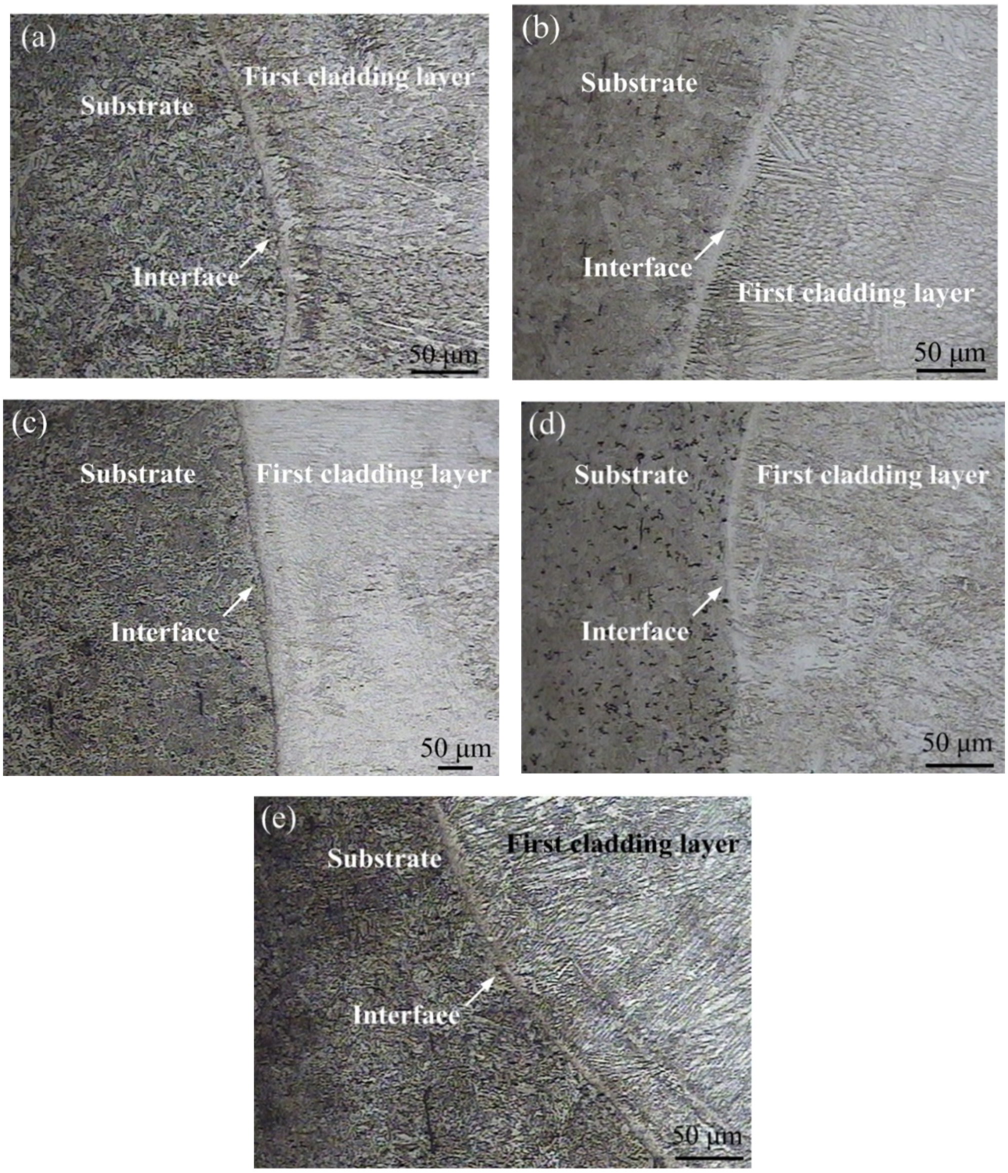

Figure 3. Photomicrograph of the lower cladding layer of different heat input, (a)~(e) were sample 1~sample 5, respectively.

Figure 4 showed the microstructure between the first layer and the second layer of cladding at different line energies. It could be seen that the location between the first and second layers of the five sample also had a good metallurgical combination. The second layer of cladding was still growing as columnar crystal. However, there was a certain Angle between the growth direction and the columnar crystal of the first layer. The growth direction of the columnar crystal of the second layer was almost perpendicular to the fusion line of the first layer and the second layer. Because the cooling gradient in this direction was the largest. It could be seen that the grain size of the second cladding layer still showed a trend of gradual decrease with the decrease of line energy. A pore defect of about 120 μm in diameter appeared in figure 4 (b), which was caused by poor argon gas protection during the cladding process.

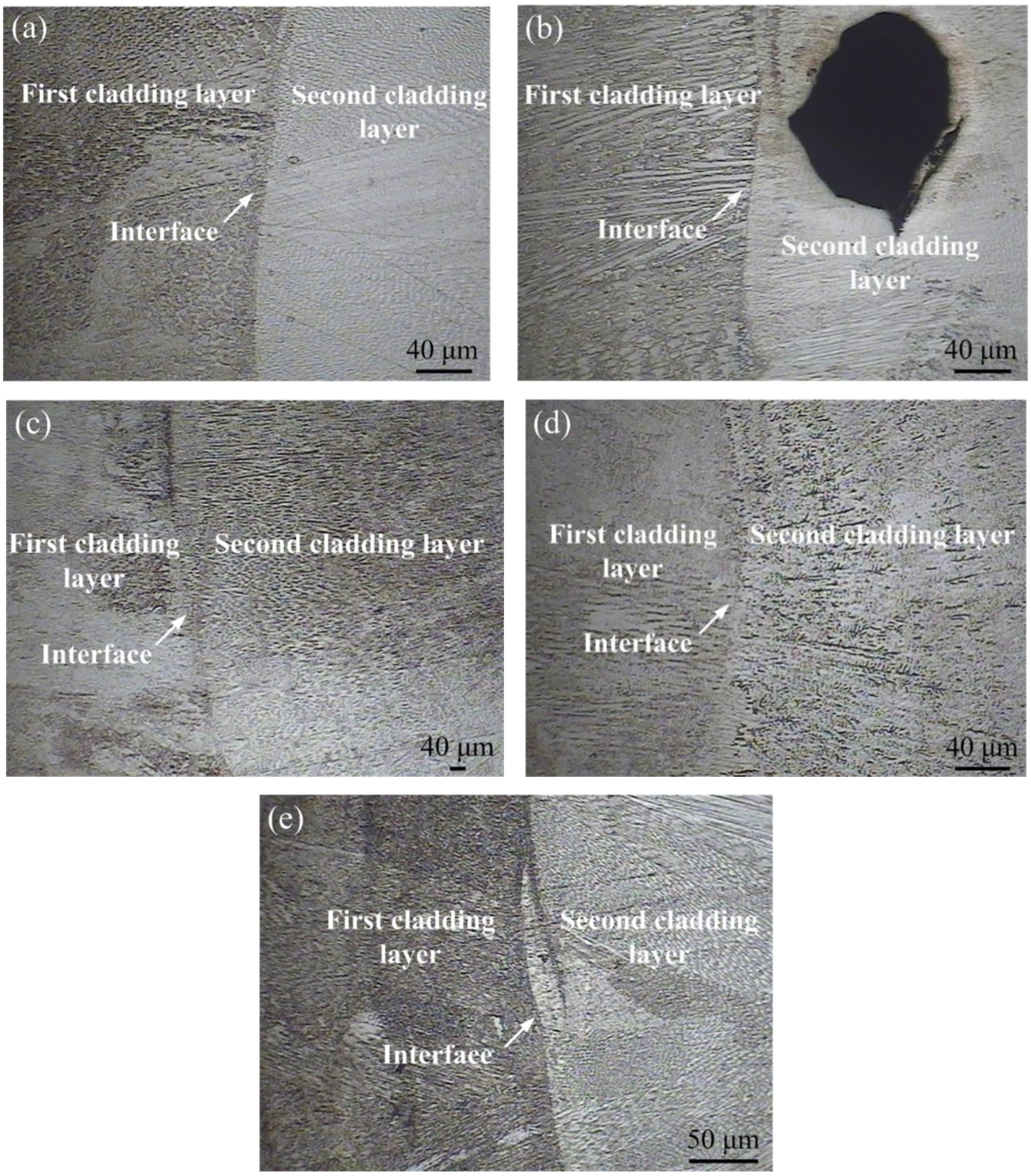

Figure 4. Photomicrograph of interlayer position of cladding layer of different heat input, (a)~(e) were sample 1~sample 5, respectively.

Figure 5 showed the microstructure of the middle part of the sample at different line energies. It could be seen that the position of the middle portion of the cladding layer of the sample 1 was mainly columnar crystals, and the columnar crystal size was large at this time. As the linear energy decreased, the cooling rate was improved, and the smaller columnar crystals appeared in the middle of the sample 2. As the linear energy decreased, the columnar crystal size also decreased. As shown in figure 5 (e), when the line energy was reduced to 530.5 J/mm, the finest columnar crystals were obtained.

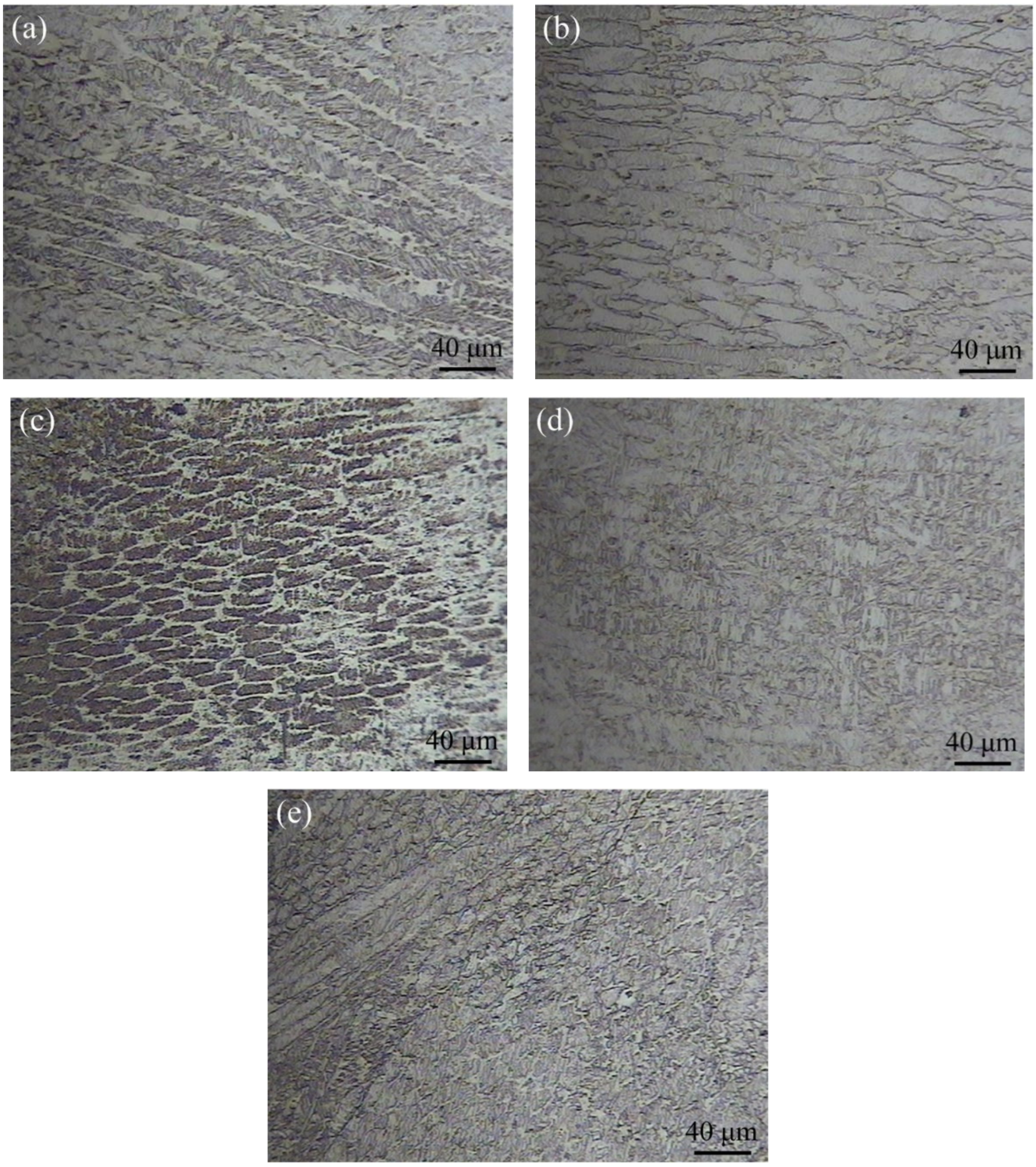

Figure 5. Photomicrograph of the middle of cladding layer of different heat input, (a)~(e) were sample 1~sample 5, respectively.

Figure 6 showed the microstructure of the upper part of the sample at different line energies. It could be seen that the upper part of the weld was mainly composed of dendrites, with a certain amount of fine grains of δ ferrite distributed around. During the solidification process, the temperature gradient in this region was large, and the dendrites grew along the maximum direction of the cooling gradient. The fine δ ferrite was due to the peritectic transformation of the primary δ ferrite and the liquid metal during welding, and was precipitated and formed from γ austenite under the action of rapid cooling. As shown in figure 6 (c) and figure 6 (e), the top of the cladding layer consisted mainly of equiaxed crystals. Because in the late stage of crystal solidification, the temperature in the central region was uniform. When the temperature drops below the freezing point, the surrounding dendrites broke into the center of the weld and grew nucleation. As the line energy decreased, the dendrite size became finer and the dendrite spacing decreased. The equiaxed crystal size at the top was also slightly reduced.

IOP Conf. Series: Earth and Environmental Science **237** (2019) 032096 doi:10.1088/1755-1315/237/3/032096

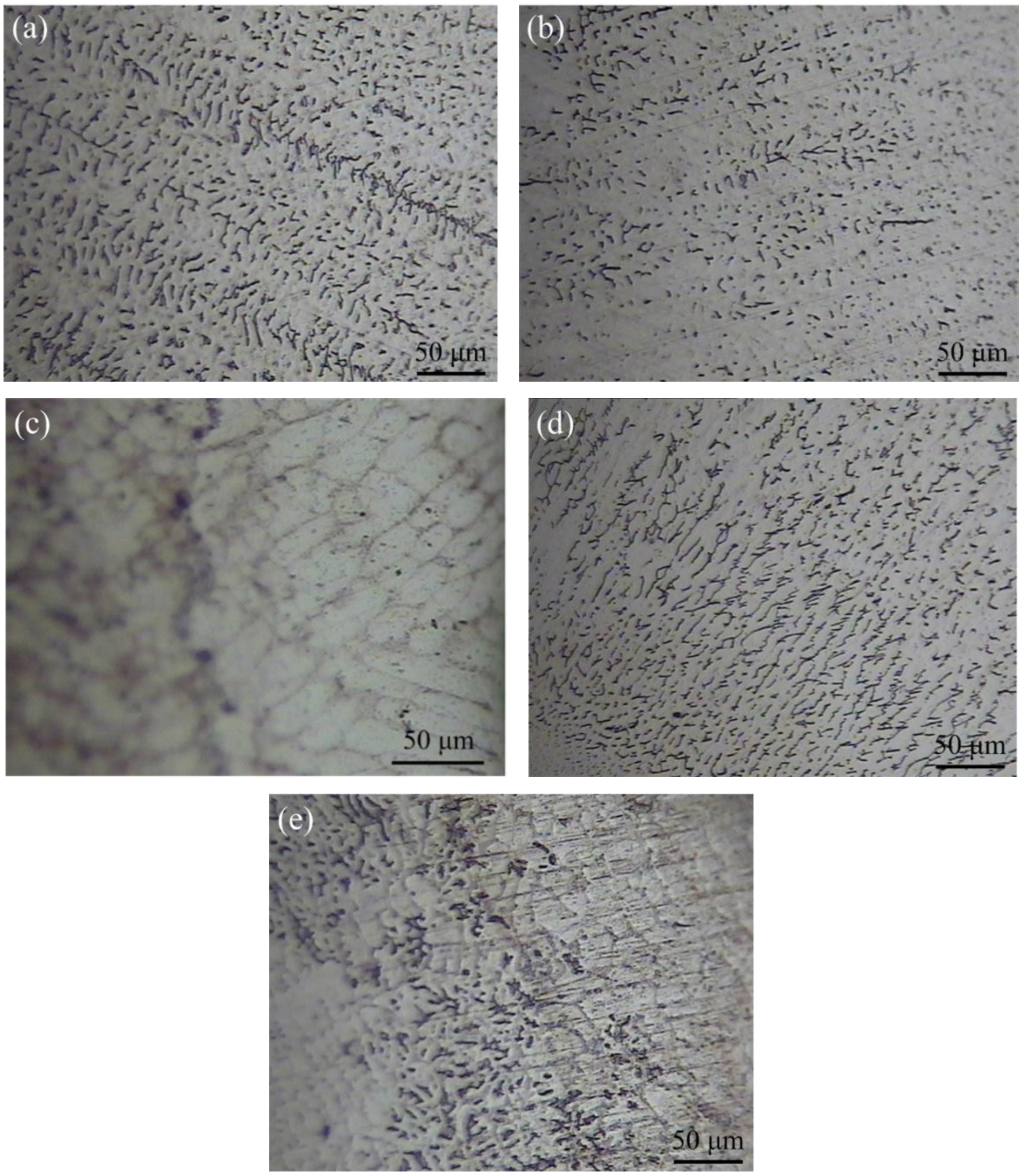

Figure 6. Photomicrograph of the upper of cladding layer of different heat input, (a)~(e) were sample 1~sample 5, respectively.

3.3. Microhardness analysis of cladding layer

The hardness distribution curve on the central line of the cladding layer under different line energy were shown in figure 7. It could be seen that under different line energy conditions, the hardness values of the three parts of the cladding layer had little difference, and they were all around 200 HV. As the line energy was gradually reduced, the hardness value of the cladding layer increased. This was because as the line energy decreases, the cladding layer structure become finer. According to the fine-grain strengthening mechanism, the finer the crystal grains, the more grain boundaries, the stronger the resistance to external deformation, and the higher the strength and hardness values.

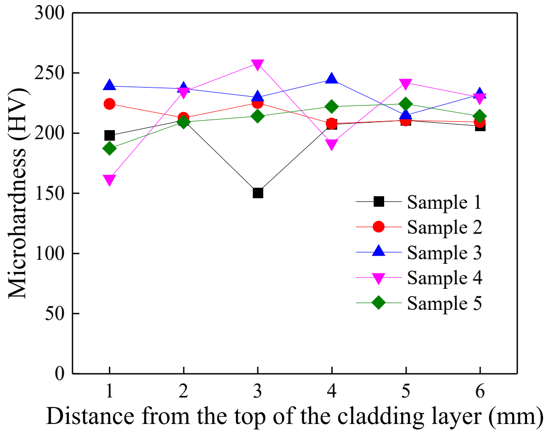

Figure 7. Comparison curve of hardness distribution law of different heat input.

4. Conclusion

In this paper, a single channel multilayer 304 stainless steel cladding layer was manufactured by using MIG filament-adding manufacturing technology, and the effect of line energy on the microhardness of the cladding layer was studied, and the following conclusions were obtained:

(1) MIG wire filler and additive manufacturing process was adopted to successfully realize the manufacturing of multilayer cladding of 304 stainless steel welding wire. The forming component of the additive manufacturing was characterized by the fact that the highest intermediate stable section at the starting end had a uniform flatness and a minimum end.

(2) The structure of the cladding layer was characterized by columnar crystals in the lower and middle part, dendrites in the upper part and equiaxed grains on the top. The structure of the cladding layer was more refined as the thermal input gradually decreased.

(3) The microhardness increased as the heat input decreased. In this paper, the highest hardness value was 257.8 HV. The process parameters were voltage 27 V, current 190 A, deposition speed 8.69 mm/s, wire feeding speed 7 m/min, wire feeding angle 90° and shielding gas flow rate 15 L/min, respectively.

References

[1] Ngo T. D., Kashani A., Imbalzano G., Nguyen K. T.Q., Hui D. (2018) Additive manufacturing (3D printing): A review of materials, methods, applications and challenges. Compos. Part B: Eng., 143:172-196.

[2] Busachi A., Erkoyuncu J., Colegrove P., Martina F., Watts C., Drake R. (2017) A review of Additive Manufacturing technology and Cost Estimation techniques for the defence sector. CIRP J. Manuf. Sci. Techn., 19: 117-128.

[3] Herzog D., Seyd V.a, Wycisk E., Emmelmann C. (2016) Additive manufacturing of metals. Acta. Mater., 117: 371-392.

[4] Srinivas M., Babu B. S. (2017) A Critical Review on Recent Research Methodologies in Additive Manufacturing. Mater. Today: Proc., 4: 9049-9059.

[5] Bourell D., Kruth J. P., Leu M., Levy G., Rosen D., Beese A. M., Clare A. (2017) Materials for additive manufacturing. CIRP Ann.-Manuf. Techn., 66: 659-681.

[6] Polonsky A. T., Echlin M. P., Lenthe W. C., Dehoff R. R., Kirka M. M., Pollock T. M. (2018) Defects and 3D structural inhomogeneity in electron beam additively manufactured Inconel 718. Mater. Charact., 143: 171-181.

[7] Aboulkhair N.T., Everitt N.M., Ashcroft I., Tuck C. (2014) Reducing porosity in AlSi10Mg parts processed by selective laser melting. Addit. Manuf., 1-4: 77-86.

[8] Murr L.E., Gaytan S.M., Ramirez D.A., Martinez E., Hernandez J., Amato K.N., Shindo P.W., Medina F.R., Wicker R.B. (2012) Metal Fabrication by Additive Manufacturing Using Laser and Electron Beam Melting Technologies. J. Mater. Sci. Technol., 28: 1-14.

[9] Cunningham C. R., Flynn J. M., Shokrani A., Dhokia V., Newman S. T. (2018) Invited review article: Strategies and processes for high quality wire arc additive manufacturing. Addi. Manuf., 22: 672-686.

[10] Wu B., Pan Z., Ding D., Cuiuri D., Li H., Xu J., Norrish J. (2018) A review of the wire arc additive manufacturing of metals: properties, defects and quality improvement. J. Manuf. Process., 35: 127-139.

[11] Xu X., Ganguly S., Ding J., Guo S., Williams S., Martina F. (2018) Microstructural evolution and mechanical properties of maraging steel produced by wire+arc additive manufacture process. Mater. Charact., 143: 152-162.